Sequence Analysis of the cbb_3 Oxidases and an Atomic Model for the *Rhodobacter sphaeroides* Enzyme†

Vivek Sharma, Anne Puustinen,‡ Mårten Wikström, and Liisa Laakkonen*

Helsinki Bioenergetics Group, Programme for Structural Biology and Biophysics, Institute of Biotechnology, University of Helsinki, PB 65 (Viikinkaari 1), FIN-00014 Helsinki, Finland

Received January 26, 2006; Revised Manuscript Received March 3, 2006

ABSTRACT: The cbb_3-type oxidases are members of the heme-copper oxidase superfamily, distant by sequence comparisons, but sharing common functional characteristics. To understand the minimal common properties of the superfamily, and to learn about cbb_3-type oxidases specifically, we have analyzed a wide set of heme-copper oxidase sequences and built a homology model of the catalytic subunit of the cbb_3 oxidase from *Rhodobacter sphaeroides*. We conclude that with regard to the active site surroundings, the cbb_3 oxidases greatly resemble the structurally known oxidases, while major differences are found in three segments: the additional N-terminal stretch of ca. 60 amino acids, the segment following helix 3 to the end of helix 5, and the C-terminus from helix 11 onward. The conserved core contains the active site tyrosine and also an analogue of the K-channel of proton transfer, but centered on a well-conserved histidine in the lower part of helix 7. Modeling the variant parts of the enzyme suggests that two periplasmic loops (between helices 3 and 4 and between helices 11 and 12) could interact with each other as a part of the active site structure and might have an important role in proton pumping. An analogue of the D-channel is not found, but an alternative channel might form around helix 9. A preliminary packing model of the trimeric enzyme is also presented.

Heme-copper oxidases are key metabolic enzymes in aerobic prokaryotes and mitochondria. They reduce molecular oxygen with electrons from catabolic reactions and generate an electrochemical gradient, which in turn drives synthesis of ATP to be used in anabolic reactions. A minimal amount of energy is lost as heat, and no reactive oxy radicals are formed (see refs *1*−*3*).

The heme-copper oxidases are large multimeric membrane proteins (*4*−*8*), characterized by their binuclear active site. An overall view of oxidase structure and function is shown in Figure 1, in the context of our cbb_3 oxidase model. The paths of the reactants and products (electrons, protons, oxygen, and water) are marked schematically to converge at the active site in the central subunit, the only subunit that is homologous in all members of the superfamily. It is approximately 500 amino acids long and forms at least 12 transmembrane helices, generally with short interhelical loops. The active site is buried deep in the helical bundle and consists of a high-spin heme (A, B, or O type) and a copper atom (Cu_B), between which the substrate oxygen binds. Cu_B is ligated by three invariant histidines, one of which is covalently bound to a unique tyrosine, which participates in the catalytic reaction (*9*) (see the detailed structure in Figure 4). The central subunit also houses a six-coordinated, low-spin heme (A or B type), which serves as the electron donor to the active site. Oxygen diffuses in through the membrane, and protons arrive to the active site via proton "channels" found in matrix/cytoplasmic side cavities of the protein. Two such channels have been characterized by site-specific mutations in bacteria and are called D- and K-channels after their central, conserved amino acids (*10*). The D-channel seems to conduct at least six of the eight protons required in the reaction, while blocking the K-channel hinders the reductive phase of the catalytic cycle in the well-studied aa_3-type oxidases (*11*, *12*). Sequence comparisons indicate identical channels in all eukaryotic and in several but not all bacterial enzymes.

The vectorial nature of reactant entry (electrons and protons) generates an electrochemical gradient across the membrane (*13*), and in addition, the enzyme is able to harness the energy released in oxygen reduction to pumping protons from inside to outside (*14*). How these two events, oxygen reduction and proton transport over the membrane, are coupled on the atomic level is still debated (*15*, *16*). What is known, however, is that all true members of the heme-copper oxidase superfamily are able to do so, while their close relatives, the nitric oxide (NO) reductases, are not (*17*, *18*). Here, by studying widely variant oxidases, we aim to explore the structural elements necessary for the coupling.

The cbb_3-type oxidases are found in various proteobacteria under microaerobic conditions (*19*). In the superfamily of heme-copper oxidases, they form a close-knit subfamily, characterized by a unique subunit composition and B-type hemes in the catalytic subunit. There are four subunits in the cbb_3-type oxidases: the catalytic subunit ccoN, which is homologous to subunit 1 of all heme-copper oxidases; the

† Support for this work was provided by the Academy of Finland (Center of Excellence, Grant 1202898) and an Academy Research Fellowship for A.P. (Grant 1200726).

* To whom correspondence should be addressed. Phone: +358-9-191-59103. Fax: +358-9-191-59920. E-mail: liisa.laakkonen@helsinki.fi.

‡ Present address: Finnish Institute of Occupational Health, Topeliuksenkatu 41 A, 00250 Helsinki, Finland.

10.1021/bi060169a CCC: $33.50
Published on Web 04/18/2006

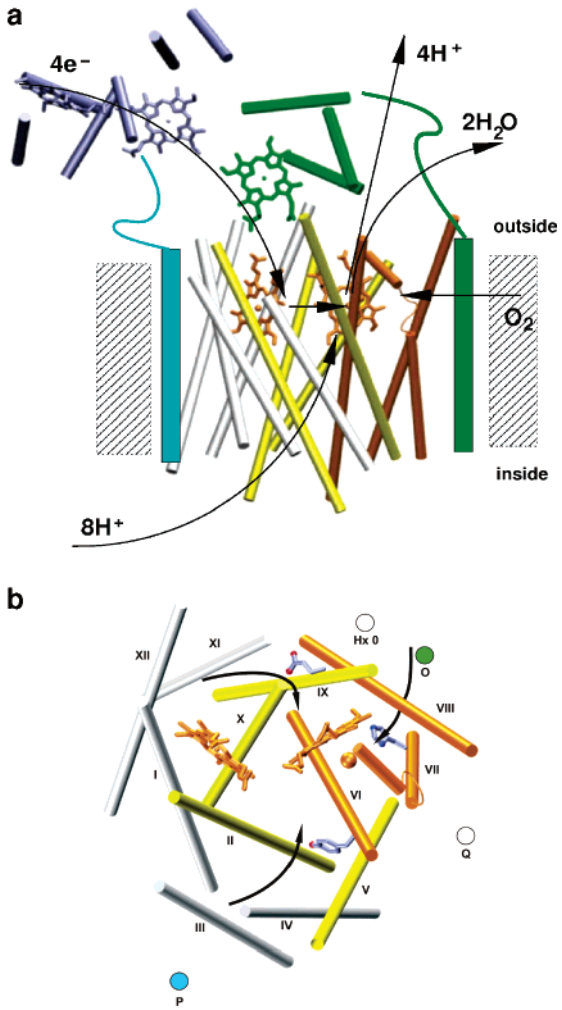

FIGURE 1: Overall view of the cbb_3 oxidase model, oriented to the membrane, from a side view (a) and a top view (b). The cytoplasm is down, and the periplasmic space is up. The catalytic subunit is shown in the middle, with helices colored according to the degree of conservation: orange for the most conserved helices, white for the least conserved, and yellow for an intermediate degree of sequence similarity. The soluble domains of subunit O (green) and subunit P (light blue) are represented by their best threading results, while the transmembrane helices are schematic. The proposed electron transfer path via all hemes in subunits P and O to the low-spin heme in the central subunit is shown. Protons and oxygen arrive, and water and protons exit from the active center on the right. The top view shows the transmembrane helices of the central subunit, rotated 90° toward the viewer. The proposed positions for the additional subunits are discussed in the text. The three putative proton channels discussed are marked with arrows, and critical residues are shown as pale blue licorice models, with side chain oxygens and nitrogens represented as red and blue spheres, respectively: Y265 in helix 6, H303 in helix 7, and E383 in helix 9.

probable immediate electron donor ccoO (*20*), which is a membrane-anchored monoheme protein; ccoP, a membrane-anchored diheme protein; and ccoQ, comprised of a single transmembrane helix (*21*) (see Figure 1). Both subunits O and P have been suggested to be part of the electron transfer chain, while the role of subunit Q is unknown (*20*, *22*−*24*). Thus, compared to the canonical oxidases, the cbb_3 oxidases lack the homologues of subunits 2 and 3, as well as the bimetallic Cu_A center, which is the electron entry point from cytochrome *c*.

It is also to be noted that the cbb_3-type oxidases differ drastically from the canonical oxidases by being catalytically promiscuous: they can reduce both O═O and N═O, as can the NO reductases (*25*, *26*). The two subunits of the NO reductases, NorB and NorC, are clearly homologous to subunits N and O of the cbb_3-type oxidases, except that the non-heme metal in the active site of NO reductases is an iron (Fe_B). Subunits P and Q are unique to the cbb_3-type oxidases.

All experimental data assert that the cbb_3 oxidases function in a manner analogous to that of the much better known aa_3-type oxidases. It follows that in addition to the similar redox centers in the catalytic subunit, one expects the presence of at least one proton channel, if not two, and also a residue similar to the Glu242 in the bovine enzyme, to guide protons either to the binuclear center, to be consumed in oxygen reduction, or to the pump site (*27*, *28*). However, nothing is known about proton channels in the cbb_3 oxidases. The extremely low degree of conservation between the different protein subfamilies presents a possibility to identify shared structural features that are perhaps from a different part of the overall structure but serve the same function of coupling electron transfer and proton transport.

A sequence comparison of the catalytic subunits shows that the cbb_3-type oxidases are divergent from both the typical aa_3-type oxidases and the aberrant ba_3-type oxidases. Very few amino acids are conserved in the whole superfamily, besides the six invariant histidines ligating the metal atoms, as verified by point mutations (*29*). Few other sites have been studied (*29*), and a functional role was assigned only to an active site tyrosine in helix 7, Y255 in *Vibrio cholerae*, corresponding to Y311 in *Rhodobacter sphaeroides* (*30*). There are no direct structural data, and not even the number of transmembrane helices is known: 12 or 13 transmembrane helices have been proposed, or 12 transmembrane helices with two prehelices lying at the membrane surface (*21*, *31*). Also, the cbb_3 oxidases from *Campylobacterales* lack the presequences but behave otherwise like other cbb_3 oxidases (*32*, *33*). Remarkably, the loop between helices 3 and 4 is highly conserved, among both non-cbb_3 and cbb_3 oxidases, yet the motifs are starkly different. Two residues in this loop have specific roles in the aa_3 oxidases (bovine numbering): Y129 forms an H-bond to W236 in helix 6, and W126 donates an H-bond to the D-propionate of the high-spin heme. Mutation of W126 to F reduces proton pumping efficiency (*34*). This loop cannot be modeled on the basis of the existing structures, if specific interactions are not restrained to form. The same need to a priori choose which residues to align applies also to the arginines in the loop between helices 11 and 12.

We have analyzed a large, phylogenetically representative set of sequences for the catalytic subunit of heme-copper oxidases and aligned them on the basis of the existing crystal structures. Our goal is to gain structural insights into the catalytic subunit of cbb_3 oxidase from *R. sphaeroides*, in addition to the mainly evolutionary considerations already available (*35*). Homology models were constructed and found to be physically sound, in comparison to the crystal structures of membrane proteins (*36*). As in the recently presented model of the *V. cholerae* enzyme (*30*), we also locate the active site tyrosine in helix 7 (Y311 in *R. sphaeroides*). In the same conserved core area, we additionally identify an analogue for the K-channel, but centered on H303. No evidence of the D-channel can be found, but a striking, cbb_3-

specific conserved glutamate (E383) in helix 9 might be involved in proton pumping. The loops between helices 3 and 4 (loop3−4) and between helices 11 and 12 (loop11−12) are proposed to form interactions similar to those found in the structurally known oxidases, but with inverted identities. Finally, a packing model for the functional trimeric enzyme is presented.

THEORETICAL METHODS

Thousands of sequences homologous to the catalytic subunit of heme-copper oxidases are known; however, mitochondrial enzymes are highly overrepresented in the database, while deviant bacterial and archaeal oxidases are few in number. For our purposes, it is the outliers in the superfamily that are most helpful in assessing the shared features. The problem of identifying relevant sequences was overcome by using several of the known variant sequences present in earlier work (*17*, *35*) as queries, and continuing iteratively, until the results converged. Approximately 160 protein sequences were retrieved from the NCBI[1] (www.ncbi.nlm.nih.gov), as results from Protein−Protein Blast (*37*). Such a large amount of data is bound to be slightly redundant and is likely to contain errors. The crystal structures from the Protein Data Bank (*38*) are the A chains of 1EHK, 1FFT, 1V55, 1M56, and 1AR1 (*4*−*8*). The structures are highly similar: the rms deviations between Cα atoms of the transmembrane helices lie in the range of 0.7−2.9 Å, while sequence identities vary from high (81%) between the aa_3 enzymes of *Paracoccus denitrificans* and *R. sphaeroides* to low (13%) between the bo_3 of *Escherichia coli* and the ba_3 of *Thermus thermophilus*.

Multiple-sequence alignments were generated using ClustalX1.8 (*39*). Degrees of similarity between sequences from different subfamilies are too low for a direct alignment, but the results depend on which types of sequences are included and the order in which they are included. Therefore, a structural alignment was first constructed by superimposing the helical segments of chain A of the five available crystal structures, as defined by STRIDE (*40*), implemented in VMD (*41*). A secondary structure profile of *Bos taurus* aa_3 was added to the structural alignment (5pdb.aln) and was used throughout the process to emphasize structural aspects and guide the work toward physically reasonable models: to penalize long gaps in the helical segments, to set a minimum length for a transmembrane helix, and to favor membrane anchoring by helically occurring R and K (*36*).

Divergent non-cbb_3-type sequences (∼70) were added to this structural alignment by sequence-to-profile methodology (cox.aln). The positioning of the catalytic site residues was checked after each addition, and if it was found to be incorrect, sequences were re-added and re-aligned in smaller subsets. The cbb_3-type sequences (∼86) were first aligned among themselves (cbb3.aln) and then added to the previous alignment by profile-to-profile methodology (all.aln). Two segments are clearly dissimilar in the cbb_3 sequences: the segment after helix 3 untill the end of helix 5 and loop11−12. Unambiguous results could not be found on the basis of sequence data alone, but structural insights were needed, as discussed below. In these segments, separate alignments to the nitric oxide reductase sequences were also instrumental. Final alignments and the structures generated from them are available at request.

Phylogenetic trees were constructed with Phylip/proml (*42*), at various stages of the alignment. The trees were studied for robustness and for finding the variant sequences to be used as additional queries. Atomic three-dimensional structures of the cbb_3 oxidase from *R. sphaeroides* were generated with MODELLER7v7 (*43*). The prehelix was omitted from the construction (residues 1−64). The sequence to be modeled was GenBank entry 1377865 (*21*) and the structural templates were 1V55 (*B. taurus*) and 1EHK (*T. thermophilus*). These two templates were used, since they are almost equally distant from the target sequence (∼18% sequence identity) and from each other. Inclusion of all five crystal structures as templates would strongly bias the results toward aa_3 oxidases. The advantage of having two templates is that MODELLER can select the better of them, although at the cost of a larger number of restraint violations, as conflicting restraints cannot be satisfied simultaneously. Approximately 15% of MODELLER's $\phi-\psi$ restraints were unsatisfied, mainly in the loops. In all other classes, there were no complaints (<1%).

The default modeling routine of MODELLER was employed, with "Thorough Variable Target Function Schedule" and "Slow MD Annealing". In-house developed charge/topology files were used for the heme and copper systems. The actual charges on the redox active metals do not influence the results to any larger degree, because the active site surroundings are identical in all templates and thus copied directly to the model. *R. sphaeroides*, *P. denitrificans*, and bovine enzymes have been crystallized in both oxidized and reduced states, and the structures are practically identical (rmsd on all Cα atoms of <0.3 Å, for the reduced and oxidized A chain of the bovine structure). To facilitate the construction process, the high-spin heme in the 1EHK template was changed to a B-type heme. Also, the nomenclature of atoms was unified between the templates and the topology files. These changes did not affect the modeling procedure.

Five models were selected from the 50 generated each time, based on the objective function value and its restraints violation profile. The stereochemical features of selected models were assessed by PROCHECK (*44*) and MolProbity (*45*), and the structures were studied visually. The alignment-modeling procedure was iterated a few times, because of problems found in the results. The alignment was changed by ±1 position at loop regions. Specific helical restraints were added to the sites where intrahelical indels were found, and MODELLER's distance restraints were used in the last runs to keep certain proposed interactions in place. Initial runs showed that a covalent bond could form between H267 and Y311. Accordingly, restraints were set to form the bond (H267:NE2−Y311:CE2) and also to stabilize the interaction between loop3−4 and helix 6 (Y181:OH−W263:NE1). Later, additional restraints were set on E180:OE1−R471:NH1, E180:OE2−R471:NH2 and low-spin heme *b*:O1A−R115:NH1, high-spin heme *b*:O1D−W470:NE1, high-spin heme *b*:O1D−K179:NZ, and high-spin heme *b*:O2D−K179:NZ.

[1] Abbreviations: COX, cytochrome *c* oxidase; MD, molecular dynamics; NOR, nitric oxide reductase; NCBI, National Center for Biotechnology Information; PDB, Protein Data Bank; SOX, *Sulfolobus* oxidase; TMPD, tetramethylphenylenediamine.

The final models were refined by energy minimization in VMD/NAMD (*41*, *46*) for 2000 conjugate gradient optimization steps, to remove any bad contacts and to relax the system. Harmonic forces (10 kcal mol^{-1} $Å^{-2}$) were applied on the backbone atoms, on the hemes, and on Cu_B. The packing of refined structures was analyzed by ANOLEA (*47*). Water molecules were added with DOWSER (*48*), and the structures were simulated with NAMD, as a test for stability. Data on internal water networks are not shown, because they are highly dependent on the detailed structure of the helices. Before several aspects of the models can be tested experimentally, conclusions from water positions would be overly hypothetical, and possibly misleading.

As a test for the modeling protocol, one of the templates (1V55, chain A) was back-modeled from the same alignment and with identical parameters, using 1EHK and one model structure as templates. The results show that the protocol performs as expected: the rmsd between the Cα atoms of the model and the actual structure was <2 Å in the helical segments.

All simulations were run on a local computer running with Red Hat Linux 9 on a 2.4 GHz Intel Xeon Processor (1GB RAM). The approximate time for one simulation round was 10 h.

Subunits O and P of *R. sphaeroides* cbb_3 oxidase were subjected to threading trials (*49*), and the best matches found for them are 1H31:B (*50*) and 1ETP:A (*51*), respectively. These were used as templates for MODELLER.

EXPERIMENTAL METHODS

Bacteriophage vector M13mp18 containing a 2.26 kb HindIII−SacI fragment from the *cco*NOQP operon encoding subunit N of *R. sphaeroides* cytochrome cbb_3 (*21*) was used as a template for site-directed mutagenesis (*52*) of key amino acid residues in subunit N of cbb_3-type oxidase. A histidine tag was added to the C-terminus of subunit *cco*N, which enables isolation of the enzyme in one step, using a metal chelate affinity column and elution with an imidazole gradient (V. Rauhamäki and A. Puustinen, manuscript in preparation). Mutations were confirmed by DNA sequencing (ABI PRISM 310 Genetic Analyzer, Applied Biosystems) throughout all processing stages, as well as from cultivations to the early stationary phase of growth in succinate minimal medium.

Activity was measured by recording oxygen consumption using a Clark-type oxygen electrode. The wild-type activity was ∼500 e^- s^{-1} (cytochrome $cbb_3)^{-1}$ using 50 mM phosphate buffer (pH 6.5) supplemented with 0.05% dodecyl maltoside, 34 μM horse heart cytochrome *c*, 0.6 mM TMPD (tetramethylphenylenediamine), and 3 mM ascorbate. Proton pumping was assessed in spheroplasts with succinate as the substrate (*21*).

RESULTS

Our concrete result is a large alignment which yielded five slightly different models of the cbb_3 oxidase from *R. sphaeroides* (rspn_12.pdb, rspn_16.pdb, rspn_30.pdb, rsnp_35.pdb, and rspn_36.pdb). Its sequence is <20% identical to the known structures, which is far below the commonly suggested limit of 40% sequence identity for the success of comparative modeling (*43*). However, the general structural relationship between all heme-copper oxidases has been clearly established (*17*, *35*), and therefore, the construction of atomic models of the cbb_3 oxidase is feasible. It is known that structurally conserved features are best evident in a large sequence comparison (*53*). Accordingly, we wanted to construct a wide, phylogenetically representative alignment of the heme-copper oxidase superfamily. The sequence space was searched thoroughly for highly divergent non-cbb_3 oxidases, because aligning these variant oxidases to the structural alignment strongly guides the later addition of the cbb_3 sequences. The reliability in aligning the aberrant oxidases is largely due to the presence of the *T. thermophilus* ba_3 enzyme in the structural alignment. Without the structural data, the *Thermus* enzyme would have aligned incorrectly with the other structurally known sequences for half of the helices. Now, with the correspondencies certain from the structural comparison, it adds extremely valuable variability to the alignment. For example, the lack of residues defining the known proton channels in the cbb_3 oxidases is not surprising, as they are also not found in the ba_3 oxidases. The non-cbb_3 sequences were aligned three times to the structural profile, to assess the robustness of the results. The match is most labile for helix 5: results vary by up to 11 residues depending on the order and the identity of the sequences that are added. The procedural details of the alignment are of utmost importance, as the modeling results are totally dependent on the underlying alignment. Finally, the aligned cbb_3 sequences matched well with the previous alignment.

The outcome of the sequence work follows closely, but not exclusively, known biological grouping: oxidases that share the same heme types are usually closest to each other, but for example, the bo_3 and aa_3 oxidases interdigitate. A continuum of sequences is a good starting point for the purposes of comparative modeling, as gradual changes from one subfamily to another can be followed more reliably than abrupt ones. The final alignment was pruned for readability and is shown in Figure 2. Figure 3 shows the phylogenetic tree derived from the alignment. It is rewarding how evenly the sequence space is divided throughout. The tree emphasizes the close relationship within the cbb_3 subfamily and justifies the choice of the templates: the bovine aa_3 sequence and the *Thermus* ba_3 sequence are far from each other, and from the cbb_3 sequences. The three crystal structures not used here as templates would fall too close to each other.

Sequence details are presented below, first for shared features in the superfamily, followed by specifics for the cbb_3 subfamily. Functionally relevant structural issues are discussed separately in the next section. In particular, we want to identify amino acids whose roles could be tested experimentally.

Invariant Residues. Besides the six histidines defining the heme-copper oxidases, there are very few highly conserved amino acids, merely a valine and a tryptophan in the active site and an arginine in loop11−12 (see Table 1 and Figure 2). Our alignment highlights several additional residues, specifically a proline in helix 8 and a glycine in helix 9, found in all but *Sulfolobus* SoxB sequences (P342 and G384 in *R. sphaeroides* cbb_3 oxidase). G384 packs extremely close to the porphyrin B-ring of the high-spin heme, which is indicative of a very similar arrangement of the whole catalytic site. P342 in helix 8 is in the immediate area of a potential proton channel, as discussed below. We also

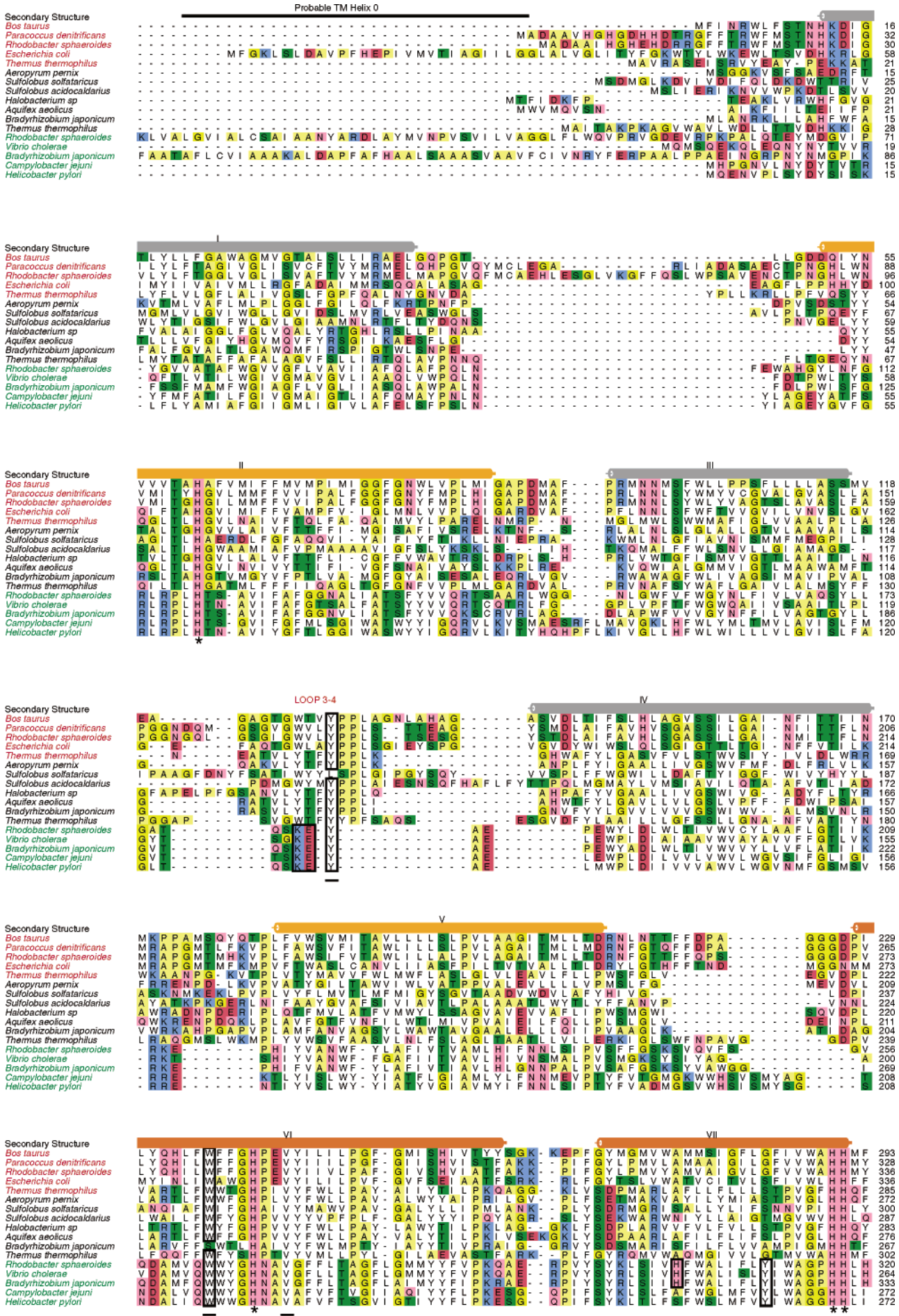
Probable TM Helix 0
I
II
III
IV
V
VI
VII
LOOP 3-4
Secondary Structure
Bos taurus
Paracoccus denitrificans
Rhodobacter sphaeroides
Escherichia coli
Thermus thermophilus
Aeropyrum pernix
Sulfolobus solfataricus
Sulfolobus acidocaldarius
Halobacterium sp
Aquifex aeolicus
Bradyrhizobium japonicum
Thermus thermophilus
Rhodobacter sphaeroides
Vibrio cholerae
Bradyrhizobium japonicum
Campylobacter jejuni
Helicobacter pylori

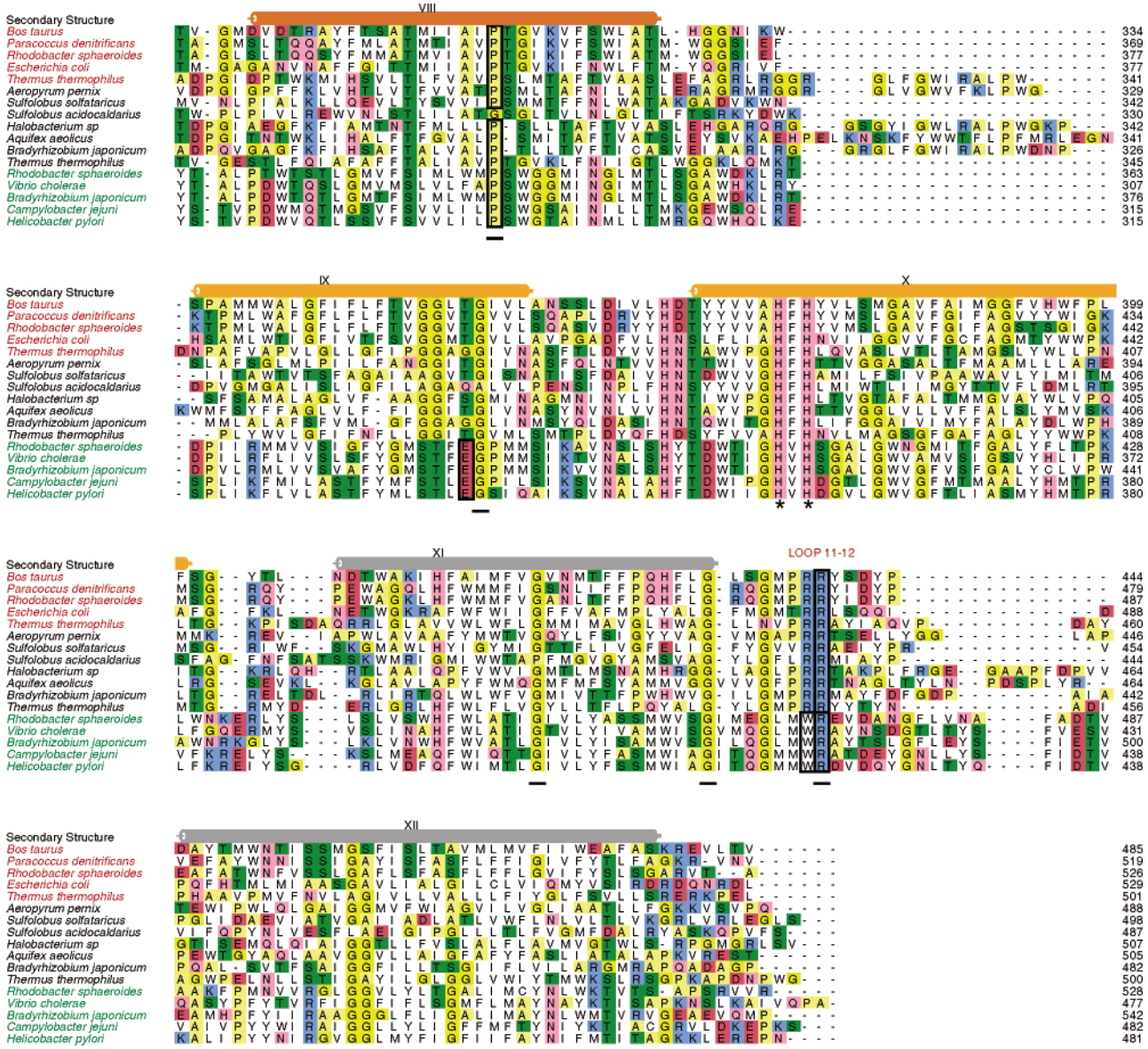

FIGURE 2: Sequence alignment of a representative set of oxidases. Names of organisms with structurally known oxidases are colored red, divergent oxidases black, and cbb_3 sequences green. The transmembrane helices are shown with the same colors as in Figure 1. Amino acids are colored by their identity. Fully conserved residues are marked with an asterisk; highly conserved residues are underlined, and those discussed in detail are boxed.

propose that a tyrosine is conserved in the otherwise divergent loop3−4 (see below).

Intrahelical Gaps. Helix 2 winds tighter in the *E. coli* and *T. thermophilus* enzymes than in the other structures, which produces a well-localized intrahelical gap in the structural alignment. Similar gaps are seen in the wider alignments. In the cbb_3 sequences, helices 4, 6, and 11 have an insertion relative to the crystal structures and helices 1, 2, and 5 a deletion, each one residue long. All are well-justified from the alignment. For example, the gap position selected in helix 6 maintains the match to bovine F251 and G252 throughout the superfamily. Omitting the indels in the model construction would result in shifting of the helical faces and produce erroneous helix−helix interactions. Initial modeling of these segments produced strangely displaced helices, but the situation was remedied by the use of MODELLER's alpha restraints.

Helical Faces. The first and last of the helices, 1 and 12, lack conserved amino acids. However, they show conserved small amino acids at α-helical periodicity (Figure 2). Structurally, this corresponds to conserved tight packing interfaces between helices 1 and 2, and between helices 12 and 11. This observation guided our alignment to results clearly different from those previously published (*17*, *30*, *35*). Similarly, helix 8 shows a conserved face toward the second helix of the canonical subunit 2, indicating that some other transmembrane helix should pack here in the cbb_3-type oxidases.

Holoenzyme. The complete cbb_3 oxidase with its four subunits has three or four additional transmemembrane helices, packed around the 12 core helices of the catalytic subunit. Some inferences to their positions can be deduced from the alignment in a structural context. The position adjacent to helix 7 is occupied in all crystal structures, although differently: by subunit 4 in the bacterial aa_3 enzymes, by the 13th helix in the *Thermus* oxidase, and by a crystallographically stable cardiolipin molecule in the bovine structure. We assume that this observation has a

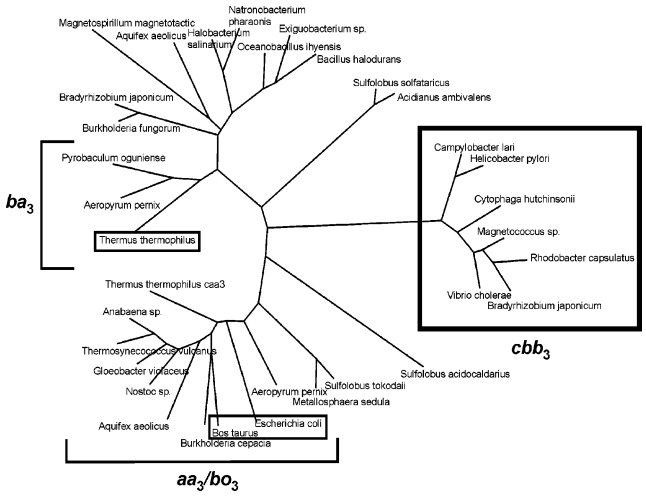

FIGURE 3: Phylogenetic tree of heme-copper oxidases, pruned for readability. Groups of different oxidases are marked. The aa_3 and bo_3 oxidases are close to each other; the variant bacterial and archaeal oxidases are separate from them (some with ba_3 hemes and others with modified A- and O-type hemes), and the cbb_3 oxidases form a totally isolated subfamily, boxed with a thick line. Three of the structurally characterized enzymes are in small boxes. The aa_3 oxidases from *P. denitrificans* and *R. sphaeroide*s are not shown on the graph, as they would completely overlap with the bovine sequence.

functional meaning, most likely related to the deformed helix 7, and its crucial role in the catalytic site. As a corollary, we suggest that the corresponding area is occupied in the cbb_3 oxidases, too, and that subunit Q would pack here (*54*; see Figure 1b for a top view of the helix packing). Both the bacterial fourth subunit and subunit Q are single-pass helices of the same polarity, even though no sequence similarity can be observed. Also occupied in all known structures are the sites of the helices of the canonical subunit 2. By weak sequence homology, we suggest that the transmembrane helix of subunit O takes the place of the second helix, packing toward helix 8 of the catalytic subunit (V. Sharma, unpublished observation). In this arrangement, heme *c* of subunit O could easily come to the same area where Cu_A is in the canonical oxidases. This agrees with measurements that show similar rates of electron transfer from heme *c*/Cu_A to the low-spin heme in the homologous proteins NO reductases and aa_3-type oxidases (*55*). Sequence analysis suggests that the N-terminal extra helix of subunit N, called helix 0 here, would form one long, kinked helix. Its polarity matches that of the first helix of the canonical subunit 2. Both helix 0 and the first helix of canonical subunit 2 are missing in some oxidases. The fourth area that most probably accommodates an extra transmembrane helix in all oxidases is next to helix 3 of the catalytic subunit. This helix has a rather conserved FW sequence motif throughout all oxidases. These two residues pack tightly to each other and seem to form the core of a hydrophobic cluster toward the first helix of subunit 3 in the bovine structure. The same sequence feature is also found in the cbb_3 oxidases, although they lack the canonical subunit 3, suggesting that some other helix would pack here. By elimination, we place the transmembrane helix from subunit P here. In this arrangement, the globular heme domains of subunits O and P are able to pack toward each other above the catalytic subunit (see Figure 1a), in a manner enabling electron transfer. As is obvious from Figure 1b, all additional helices gather around the conserved half of the catalytic subunit, suggesting that the integrity of the active site requires the extra helices.

Homology modeling fails for segments that show major divergence. With regard to the cbb_3 oxidases, this means loop3−4, loop11−12, and helices 4 and 5. In the crystal structures, the two loops come in contact with the hemes, and certain residues have been shown to have functional roles (*34*, *56*, *57*). As a result, all heme propionates participate in polar interactions with protein residues. A similar situation was considered a goal for the homology modeling and was satisfied (Table 2). For these nonhomologous areas, specific attention was paid to locating meaningful interactions, which could then be imposed by restraints in the model construction. In the crystal structures, the interface between helices 4 and 5 is stabilized by polar interactions. The residues in question are not found in the cbb_3 oxidases, but there are other invariant residues that can form analogous interactions, as discussed below.

Loop3−4. In several publications, helix 4 is aligned by the C-terminal basic residues (*17*, *30*). The number of inserted gaps varies (*17*), and the helices are different in length (*30*). The highly conserved motif (**W/Y**xxYPPL) in loop3−4 of the non-cbb_3 oxidases is left completely unmatched by the cbb_3 oxidases (*35*), or a match is made to the C-terminal, variable part of the loop (*30*). Still, there are experimental data indicating that the N-terminal, conserved part of the loop is functionally important (*34*). In all crystal structures, a W/Y at the innermost point of loop3−4 forms an H-bond to the D-propionate of the high-spin heme, and the conserved tyrosine after it hydrogen bonds to an invariant tryptophan in helix 6, which in turn stacks to one of the helix 7 Cu_B ligand histidines. A conserved tyrosine is found also in the corresponding loop of the cbb_3 sequences. We chose to maintain the interaction to the conserved oxidase core: loop3−4:Y−helix6:W−helix7:H. The analogous Y181−W263 interaction was constrained to form in the cbb_3 models. This brings the residues preceding this tyrosine to the tip of the loop, and into interaction with the catalytic site. This specific structural match has not been suggested before, and if it is indeed real, the tyrosine is one of the very few completely conserved residues in the superfamily, and presumably of importance in maintaining the active site structure. The well-conserved basic residue in the **K/R**EY motif in loop3−4 of the cbb_3 oxdases will now interact with the D-propionate of the high-spin heme, while the A-propionate interacts with N393 and H397 from a conserved stretch preceding helix 10, similarly as in the known structures. Table 2 shows all propionate−protein interactions. As a result of the restrained interactions mentioned in Table 2, helix 4 in the cbb_3 oxidases becomes rather short, and two conserved acids are forced into the helix. Variation in the lengths of helices is observed when comparing *Thermus* oxidase to the bovine enzyme. The conserved acidic residues, E185 and D189, point toward helix 5 (see below). Loop3−4 is homologous between the cbb_3 oxidase and the NO reductases, some of which (e.g., *Thiobacillus denitrificans*, *Azoarcus* sp., and *Photobacterium profundum*) have an insertion before the proposed helix start, supporting the suggested model for loop3−4 and helix 4 (data not shown).

Loop11−12. The cbb_3 oxidases also differ from the other members of the superfamily with respect to loop11−12.

Table 1: Conserved Amino Acids in the Heme-Copper Oxidase Superfamily

type or location	*B. taurus* (aa_3)	*T. thermophilus* (ba_3)	*R. sphaeroides* (cbb_3)
invariant metal ligands			
low-spin heme Fe	H61, H378	H72, H386	H118, H407
high-spin heme Fe	H376	H384	H405
Cu_B	H240, H290, H291	H233, H282, H283	H267, H317, H318
active site			
loop3−4	Y129	Y136	Y181
loop11−12	R439	R450	R471
helix 6	W236	W229	W263
helix 6	V243	V236	V270
other conserved residues			
helix 8	P315	P308	P342
helix 9	G355	G363	G384
helix 11	G420	G431	G451
helix 11	G432	G443	G463
subfamily-specific functionally important residues			
D-channel	D91, E242	−	−
K-channel	K319	−	H303[a]
His-Tyr	Y244	Y237	Y311[b]

[a] Forming an analogous channel. [b] Structurally conserved, but not from the same part of the sequence.

Table 2: Interactions between Heme Propionates and the Protein

heme	propionate oxygen	interacting residue atom: *B. taurus* (aa_3)	interacting residue atom: *R. sphaeroides* (cbb_3)
a/*b*	O1A	Y54 OH, Y371 OH, Wat5[b]	R115 NH1[a]
	O2A	R439 N, Wat36[b]	R471 N
	O1D	W126 N	K179 N
	O2D	R439 NE, Wat36[b]	R471 NE
a_3/b_3	O1A	D364 OD2, H368 ND1	N393 ND2, H397 ND1
	O2A	H368 ND1, Wat34,[b] Wat16[b]	H397 ND1
	O1D	R438 NH1, Wat34,[b] Wat44[b]	W470 NE1,[a] K179 NZ [a]
	O2D	R438: NH2, W126 :NE1	K179 NZ[a]

[a] Atoms that are restrained to form interactions with respective heme propionates. [b] Wat is a crystallographic water molecule.

Instead of the widely studied conserved double arginine (bovine R438R439) (*56*−*61*), the cbb_3 oxidases have a tryptophan and an arginine, W470R471. A choice was made to match the single arginine of the cbb_3 sequences to the latter of the arginine pair of the canonical oxidases and to retain its interactions with both propionates of the low-spin heme. The A-propionate accepts a hydrogen bond from R115 (conserved grlR) at the beginning of helix 2 and from the backbone amide of R471, while the D-propionate interacts with the backbone of K179 and the loop11−12 arginine (see Table 2 and Figure 5).

Correlated Changes. Comparison of helices 4 and 5 between structures and cbb_3 sequences is hard indeed: no clear sequence motifs are found. In this area, the ba_3 oxidases are closer to the cbb_3 oxidases than to the aa_3/bo_3 oxidases, and the *T. thermophilus* structure is invaluable. For example, tryptophans 186 and 196 of *R. sphaeroides* cbb_3 oxidase have counterparts in the variant oxidases. Also, several correlated changes between the helices are observed. The central proline (P200) of bovine helix 5 and a helix 4 tryptophan (W196) in the ba_3/cbb_3 sequences show perfect mutual exclusion. Superposition of the bovine structure and the *R. sphaeroides* model shows that the two residues would collide if they coexisted. In the bovine structure, two conserved hydrogen-bonded pairs are seen between these helices (helix4:D144−helix5:R213 and helix4:H151−helix5:T207). A similar intimately connected interface is seen in the cbb_3 model, when subfamily-specific residues form a pair interaction (helix4:D189−helix5:N236). The conserved pattern is systematic and complex, lending credibility to the present alignment. A similar situation is seen between helices 11 and 12: whenever a well-conserved G in helix 12 (G500 in *R. sphaeroides* cbb_3 and G457 in bovine) is substituted with a larger amino acid (L, I, or V) its spatially nearest neighbor in helix 11 is a glycine or alanine, while the site otherwise is occupied by large hydrophobic residues (M423 in bovine and L454 in cbb_3 oxidases). Despite the initial problems, the final alignment for helix 5 is highly satisfying.

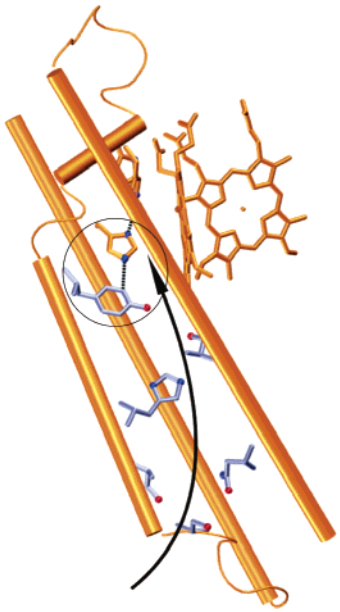

FIGURE 4: Putative K-channel analogue, centered around H303. Helices 7, 6, and 8 are shown as cylinders (from left to right) and hemes as licorice models (heme *b* on the right and heme b_3 perpendicular to the plane of the page). Colors are as in previous figures. The channel-forming residues that are shown are Y311, S343, H303, S300, N349, and S296, as counted from the top. The proton path is marked with an arrow, and the covalently bound His-Tyr pair in the active site is circled.

cbb_3-Specific Sequence Features. Besides looking for features shared in the whole superfamily, we found it to be informative to compare the cbb_3 oxidases with one another.

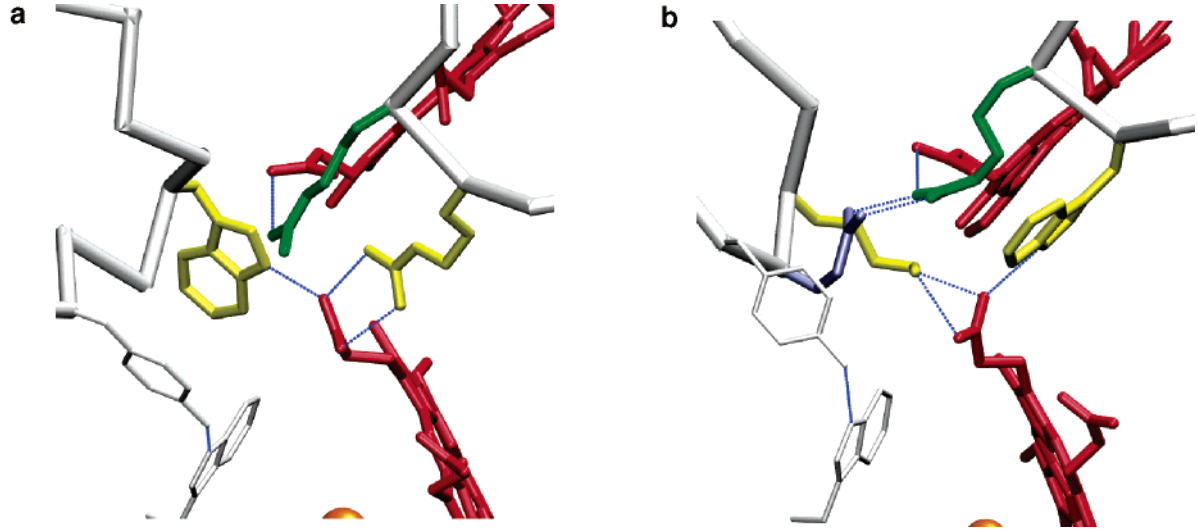

FIGURE 5: Gating residues in the bovine structure (a) and the proposed model (b) from the top. Loop3−4 is shown as a white trace at the left and loop11−12 at the right. The hemes are colored red; the conserved arginine in loop11−12 is colored green, and the tyrosine from loop3−4 that interacts with tryptophan in helix 6 is colored white. The gating residues in the bovine structure (the lower number arginine in loop11−12 and the tryptophan in loop3−4) are colored yellow, as are the proposed, inverted gating residues in the model. The glutamate in loop3−4 of the model is colored pale blue.

Table 3: Properties of Wild-Type and Mutant Cytochrome cbb_3 Enzymes from *R. sphaeroides*

	activity (% of wild type)	reduced cytochrome *c*[a]	proton translocation[b] (H^+/e^-)
wild type	100	no	2.6−3
Y311G	0	yes	ND[c]
Y311F	0	yes	ND[c]
Y265F	19	no	2.4−2.8
E383Q	1.2	no	ND[c]
E383D	30	no	2.5−2.9

[a] The three cytochrome *c* forms in the isolated enzyme are reduced in the as isolated minus air spectra, indicating that electrons are not transferred to the binuclear center. [b] Two of the observed H^+/e^- are released from the cytochrome bc_1 complex; thus, the wild-type cytochrome cbb_3 shows a H^+/e^- ratio close to unity. [c] Not determined.

One acidic residue is especially noticeable: E383 is fully conserved among the cbb_3 oxidases, and it is the only such residue predicted to lie clearly within the membrane domain. It is situated in the middle of transmembrane helix 9, and it lacks obvious possibilities of forming ionic interactions. A possible functional role of E383 was tested by mutations to both Q and D. The more conservative E to D mutation retained approximately one-third of the activity of the wild type, with a normal H^+/e^- ratio of proton translocation, while the E to Q mutant was virtually inactive (Table 3). The proposed active site tyrosine, Y311, was also tested for its role in catalysis. Mutation to phenylalanine yielded a completely inactive enzyme, as found in ref *27*. Y265 was mutated to phenylalanine to test whether it might be analogous to the tyrosine in *Rhodothermus marinus* that is part of the D-channel (ref *62* and Table 3). The modest inhibition of turnover and the essentially normal efficiency of proton translocation do not support this possibility. However, we cannot exclude the possibility that a functional role of this tyrosine might have been taken over by water molecules.

DISCUSSION

The cbb_3 oxidases form the most distant subgroup among heme-copper oxidases. Minimal conservation is observed between them and the whole superfamily: besides the histidines, only eight of 535 residues are highly conserved in our large alignment. The built homology model is very clearly divided into the well-conserved surroundings of the active site (helices 6−10) and the variant other half of the helix bundle (see Figure 1b). In the conserved core, only few gaps are needed in the alignment, and the models are very robust. On the other hand, the detailed structure of the variant half is strongly dependent on the choices made on the alignment level and could easily vary. The core contains the active site and the K-channel, while the other proton channel, the functionally dominant D-channel in the canonical oxidases, originates in helices in the variant half. The same general result is obvious when comparing published alignments between structurally known oxidases and the cbb_3-type oxidases (*17*, *30*, *35*). All agree well for the core but show major variations for the termini. No comparison can be made with the recently published model of the cbb_3 oxidase from *V. cholerae* (*30*), as the coordinates are not available.

Core Enzyme. The heme-copper oxidase superfamily is defined by the six histidine ligands of the redox active metals, five of which are in the conserved core part of the enzyme. Notably, the active site tyrosine (*9*, *63*) from helix 6, missing only from the cbb_3-type oxidases, can easily be substituted with another tyrosine from helix 7 (see Figures 2 and 4), as also shown recently (*30*). Direct chemical verification of a covalent histidine−tyrosine adduct is still missing, but mutations of the tyrosine render the enzyme inactive (ref *30* and Table 3) as in the aa_3 oxidases (*64*). The orientation of the His-Tyr pair would be different, though, when the tyrosine is not in the same helix but in a neighboring helix. This is consistent with the different ligand dissociation behavior in the cbb_3 enzymes (*65*), indicative of changes in the shape of the active site. The interface between helices 6 and 7 is highly constrained by Cu_B ligation, and a shift of the tyrosine position is not likely to change the dynamics of the active site.

"K-Channel". A feature shared by all heme-copper oxidases but a few archae (*Sufolobus* and *Metallosphaera*)

is a central proline in helix 8 (P315 in the bovine enzyme). The proline is one turn above the lysine defining the K-channel (K319) and kinks the helix slightly, allowing for a small cavity toward helix 7. The site where the aa_3 oxidases have the K is invariantly occupied by a G in the cbb_3 oxidases, and its small side chain leaves space where a histidine, H303, is found in helix 7. H303 is conserved in all cbb_3 oxidases but those of *Campylobacterales*. The corresponding histidine from *Bradyrhizobium japonicum* has been mutated by Zufferey et al. (*29*), who report a native structure but catalytic inactivity, the only conserved histidine with this phenotype. H303 in our model is situated in the cytoplasmic half of helix 7, and around it are several conserved hydrophilic residues: S296, S300, H303, Y311, S343, and N349 (as shown in Figure 4). Remarkably, N349 aligns well with the ba_3-type oxidases, which also lack a channel-forming lysine. Other possible channel-forming residues in the *Thermus* enzyme would be D262, S261, and S309. The proposed channel looks structurally very different from the known K-channel and rather resembles the D-channel: several polar residues traverse the height of the channel, tracing a path between the helices. The uppermost residue on the suggested channel is Y311 in the active site. If the analysis of evolution in this family is accurate (*17*) and the cbb_3 oxidases are remnants of the older, more primitive enzymes, then the separation of the active site and the proton channel, as seen in aa_3 oxidases, should have served to optimize catalytic efficiency.

Variant Loops. The loops between helices are generally short in the oxidases. In contrast, the loops between helices 3 and 4 and between helices 11 and 12 both extend inward and meet above the catalytic site. Residues from both loops [bovine W126 (loop3−4) and R439 (loop11−12)] are in contact with the hemes and have been shown to participate in function (*34*, *56*−*61*). In the bovine structure, the loops also make direct contact with each other. The difference in loop3−4 is striking: both the non-cbb_3 and cbb_3 oxidases have well-conserved sequences here, though they are totally different from one another (GWTVYPPL and GKEYAE, respectively). Moreover, the ends of helices 3 and 4 are hard to discern, and in most published alignments, this loop is totally nonexistent (*30*, *35*). Loop3−4 is shorter in the cbb_3-type oxidases, especially the segment C-terminal to Y181. The only way we found to solve this problem was to shorten helix 4 and force interactions between the **KEY** motif and the heme propionate to take place. With this interaction organizing loop3−4, contacts to loop11−12 can also be found between the glutamate in the K/R**E**Y motif and the single conserved R in loop11−12. Also here an active choice was required: the loop in the canonical oxidases contains two invariant arginines, R438 and R439, but only one arginine in loop11−12 is conserved in the cbb_3 oxidases (R471). There are experimental data backing either choice (*56*, *57*, *59*), and we picked the latter one, as both cbb_3 oxidases and NO reductases have a conserved pair there, WR and QR, respectively. Following the arginine, the loop in the cbb_3 oxidases is ∼10 residues longer and well-conserved. Some non-cbb_3 oxidases also have longer than average loops between helices 11 and 12 (e.g., *Pyrobaculum aerophilum*, *Halobacterium salinarium*, and *Bacillus halodurans*); however, these loops are clearly not homologous with those in the cbb_3 oxidases, and in the structures, this loop binds to subunit 2. We suggest that the extra length of loop11−12 reaches to the area left open by the short loop3−4 in the cbb_3 oxidases and may contact subunit O or P. As a result of the restrained interactions, all heme propionates end up having polar interactions (Table 2).

The proposed role of these loops in proton pumping suggests interesting questions about the cbb_3 oxidases. Key structural elements in this domain might be inverted in the cbb_3 oxidases but contain the same elements. The D-propionate of the high-spin heme may be locked by competing interactions with a tryptophan and an arginine, as in the well-studied cases, but in the cbb_3 oxidases the locking residues may have shifted places: the R/K is in loop3−4 and the W in loop11−12, as shown in Figure 5.

D-Channel. The best understood proton channel in the canonical oxidases, the D-channel, reaches from D91 in loop2−3 to E242 of helix 6 (bovine numbering). Several amino acids between D91 and E242 mediate proton hopping, among them the well-conserved N99. These residues are all missing from the cbb_3 oxidases and also from the divergent oxidases. These two odd enzyme subgroups both have a mostly basic loop2−3 instead of hydrophobic residues surrounding Asp91 (bovine). A channel has been proposed in this area from the *T. thermophilus* ba_3 structure (*4*), but it has not been verified experimentally to the best of our knowledge. An alternative path for the proton channel has been shown to exist in the archea *Rh. marinus* caa_3 where the lack of the helix 6 glutamate is compensated by a tyrosine (*62*) two residues before the helix 6 histidine. A corresponding tyrosine (Y265) is always found in the cbb_3 oxidases, and this presents the only trace of a possible D-channel in this region. However, *Rh. marinus* does have the D and N in the lower part of helix 2, as in the canonical oxidases, but these are lacking in the cbb_3 oxidases. Mutation of Y265 diminishes the activity of *R. sphaeroides* cbb_3 oxidase but does not significantly affect the efficiency of proton pumping at the cell level (Table 3), and the importance of this residue thus remains obscure. At this time, we cannot exclude the possibility that Y265 and the domain beneath it would not be used as a proton transfer pathway, but if that is the case, the channel structure would be entirely different.

E383 in helix 9 is the only carboxylic amino acid, conserved among the cbb_3 enzymes, that is predicted to reside within the membrane domain at (or below) the level of the heme groups. Its mutation to aspartate and glutamine shows moderate and virtually complete inhibition of activity, respectively. In the former case, the efficiency of proton translocation was unaffected (Table 3). The possibility that E383 participates in proton transfer requires further experimentation, especially since its side chain points awkwardly into the membrane area in the present models. Further refinement of the model is underway, and the possibility that the conserved D364 might be involved in such a putative channel is also being tested.

In summary, combination of existing structural and sequence data on heme-copper oxidases has allowed us to construct models of the divergent members of the group, the cbb_3 oxidases, and to locate several functionally important residues, the first of which have already been verified experimentally. Consistent with the observed division of the structure into a conserved and a variant half, an analogue is found for the K-channel but not for the D-channel. This

proposes radically different proton pathways in the cbb_3 oxidases and even opens up the possibility of a primitive single-channel oxidase.

ACKNOWLEDGMENT

We thank Ms. Virve Rauhamäki for fruitful discussions.

REFERENCES

1. Ferguson-Miller, S., and Babcock, G. T. (1996) Heme/Copper terminal oxidases, *Chem. Rev. 96*, 2889−2907.
2. Babcock, G. T., and Wikström, M. (1992) Oxygen activation and the conservation of energy in cell respiration, *Nature 356*, 301−309.
3. Ostermeier, C., Iwata, S., and Michel, H. (1996) Cytochrome *c* Oxidase, *Curr. Opin. Struct. Biol. 6*, 460−466.
4. Soulimane, T., Buse, G., Bourenkov, G. P., Bartunik, H. D., Huber, R., and Than, M. E. (2000) Structure and mechanism of the aberrant ba_3 cytochrome *c* oxidase from *Thermus thermophilus*, *EMBO J. 19*, 1766−1776.
5. Abramson, J., Riistama, S., Larsson, G., Jasaitis, A., Svensson-Ek, M., Laakkonen, L., Puustinen, A., Iwata, S., and Wikström, M. (2000) The Structure Of Ubiquinol Oxidase From *Escherichia coli*, *Nat. Struct. Biol. 7*, 910−917.
6. Tsukihara, T., Shimokata, K., Katayama, Y., Shimada, H., Muramoto, K., Aoyama, H., Mochizuki, M., Shinzawa-Itoh, K., Yamashita, E., Yao, M., Ishimura, Y., and Yoshikawa, S. (2003) The low-spin heme of cytochrome *c* oxidase as the driving element of the proton-pumping process, *Proc. Natl. Acad. Sci. U.S.A. 100*, 15304−15309.
7. Svensson-Ek, M., Abramson, J., Larsson, G., Tornroth, S., Brezezinski, P., and Iwata, S. (2002) The X-ray Crystal Structures of Wild-type and EQ(I-286) Mutant Cytochrome *c* Oxidases from *Rhodobacter sphaeroides*, *J. Mol. Biol. 321*, 329−339.
8. Ostermeier, C., Harrenga, A., Ermler, U., and Michel, H. (1997) Structure at 2.7 Å resolution of the *Paracoccus denitrificans* two-subunit cytochrome *c* oxidase complexed with an antibody F_v fragment, *Proc. Natl. Acad. Sci. U.S.A. 94*, 10547−10553.
9. Wikström, M. (1989) Identification of the electron transfers in cytochrome oxidase that are coupled to proton pumping, *Nature 338*, 776−778.
10. Gennis, R. B. (1998) Multiple proton-conducting pathways in cytochrome oxidase and a proposed role for the active-site tyrosine, *Biochim. Biophys. Acta 1365*, 241−248.
11. Bloch, D., Belevich, I., Jasaitis, A., Ribacka, C., Puustinen, A., Verkhovsky, M. I., and Wikström, M. (2004) The catalytic cycle of cytochrome *c* oxidase is not the sum of its two halves, *Proc. Natl. Acad. Sci. U.S.A. 101*, 529−533.
12. Konstantinov, A. A., Siletsky, S., Mitchell, D., Kaulen, A., and Gennis, R. B. (1997) The roles of the two proton input channels in cytochrome *c* oxidase from *Rhodobacter sphaeroides* probed by the effects of site-directed mutations on time-resolved electrogenic intraprotein proton transfer, *Proc. Natl. Acad. Sci. U.S.A. 94*, 9085−9090.
13. Mitchell, P. (1961) Coupling of phosphorylation to electron and proton transfer by a chemiosmotic type of mechanism, *Nature 191*, 144−148.
14. Wikström, M. K. F. (1977) Proton pump coupled to cytochrome-c oxidase in mitochondria, *Nature 266*, 271−273.
15. Faxén, K., Gilderson, G., Ädelroth, P., and Brzezinski, P. (2005) A mechanistic principle for proton pumping by cytochrome *c* oxidase, *Nature 437*, 286−289.
16. Belevich, I., Verkhovsky, M. I., and Wikström, M. (2006) Proton-coupled electron-transfer drives the proton pump of cytochrome *c* oxidase, *Nature* (in press).
17. Hendriks, J., Gohlke, U., and Saraste, M. (1998) From NO to OO: Nitric oxide and dioxygen in bacterial respiration, *J. Bioenerg. Biomembr. 30*, 15−24.
18. Zumft, W. G. (1997) Cell Biology and Molecular Basis of Denitrification, *Microbiol. Mol. Biol. Rev. 61*, 533−616.
19. Myllykallio, H., and Liebl, U. (2000) Dual role for cytochrome cbb_3 oxidase in clinically relevant proteobacteria? *Trends Microbiol. 8*, 542−543.
20. Zufferey, R., Preisig, O., Hennecke, H., and Thöny-Meyer, L. (1996) Assembly and Function of the Cytochrome cbb_3 Oxidase Subunits in *Bradyrhizobium japonicum*, *J. Biol. Chem. 271*, 9114−9119.
21. Toledo-Cuevas, M., Barquera, B., Gennis, R. B., Wikström, M., and Garcia-Horsman, J. A. (1998) The cbb_3-type cytochrome *c* oxidase from *Rhodobacter sphaeroides*, a proton-pumping heme-copper oxidase, *Biochim. Biophys. Acta 1365*, 421−434.
22. Koch, H., Hwang, O., and Daldal, F. (1998) Isolation and Characterization of *Rhodobacter capsulatus* Mutants Affected in Cytochrome cbb_3 Oxidase Activity, *J. Bacteriol. 180*, 969−978.
23. DeGier, J. W. L., Schepper, M., Reijnders, W. N. M., VanDyck, S. J., Slotboom, D. J., Warne, A., Saraste, M., Krab, K., Finel, M., Stouthamer, A. H., VanSpanning, R. J. M., and VanderOost, J. (1996) Structural and functional analysis of aa_3-type and cbb_3-type cytochrome *c* oxidases of *Paracoccus denitrificans* reveals significant differences in proton-pump design, *Mol. Microbiol. 20*, 1247−1260.
24. Pitcher, R. S., Cheesman, M. R., and Watmough, N. J. (2002) Molecular and Spectroscopic Analysis of the Cytochrome cbb_3 Oxidase from *Pseudomonas stutzeri*, *J. Biol. Chem. 277*, 31474−31483.
25. Forte, E., Urbani, A., Saraste, M., Sarti, P., Brunori, M., and Giuffrè, A. (2001) The cytochrome cbb_3 from *Pseudomonas stutzeri* displays nitric oxide reductase activity, *Eur. J. Biochem. 268*, 6486−6491.
26. Fujiwara, T., and Fukumori, Y. (1996) Cytochrome *cb*-Type Nitric Oxide reductase with Cytochrome *c* Activity from *Paracoccus denitrificans* ATCC 35512, *J. Bacteriol. 178*, 1866−1871.
27. Michel, H. (1998) The mechanism of proton pumping by cytochrome *c* oxidase, *Proc. Natl. Acad. Sci. U.S.A. 95*, 12819−12824.
28. Verkhovskaya, M. L., Garcia-Horsman, A., Puustinen, A., Rigaud, J. L., Morgan, J. E., Verkhovsky, M. I., and Wikström, M. (1997) Glutamic acid 286 in subunit I of cytochrome bo_3 is involved in proton translocation, *Proc. Natl. Acad. Sci. U.S.A. 94*, 10128−10131.
29. Zufferey, R., Arslan, E., Thöny-Meyer, L., and Hennecke, H. (1998) How Replacements of the 12 Conserved Histidines of Subunit I Affect Assembly, Cofactor Binding, and Enzymatic Activity of the *Bradyrhizobium japonicum* cbb_3-type Oxidase, *J. Biol. Chem. 273*, 6452−6459.
30. Hemp, J., Christian, C., Barquera, B., Gennis, R. B., and Martinez, T. J. (2005) Helix Switching of a Key Active-Site residue in the Cytochrome cbb_3 Oxidase, *Biochemistry 44*, 10766−10775.
31. Zufferey, R., Thöny-Meyer, L., and Hennecke, H. (1996) Histidine 131, not histidine 43, of the *Bradyrhizobium japonicum* FixN protein is exposed towards the periplasm and essential for the function of cbb_3-type cytochrome oxidase, *FEBS Lett. 394*, 349−352.
32. Smith, M. A., Finel, M., Korolik, V., and Mendz, G. L. (2000) Characterisitcs of the aerobic respiratory chains of the microaerophiles *Campylobacter jejuni* and *Helicobacter pylori*, *Arch. Microbiol. 174*, 1−10.
33. Tsukita, S., Koyanagi, S., Nagata, K., Koizuka, H., Akashi, H., Shimoyama, T., Tamura, T., and Sone, N. (1999) Characterization of a *cb*-type cytochrome *c* oxidase from *Helicobacter pylori*, *J. Biochem. 125*, 194−201.
34. Ribacka, C., Verkhovsky, M. I., Belevich, I., Bloch, D. A., Puustinen, A., and Wikström, M. (2005) An Elementary Reaction Step of the Proton Pump Is Revealed by Mutation of Tryptophan-164 to Phenylalanine in Cytochrome *c* Oxidase from *Paracoccus denitrificans*, *Biochemistry 44*, 16502−16512.
35. Pereira, M. M., Santana, M., and Teixera, M. (2001) A novel scenario for the evolution of haem-copper oxygen reductases, *Biochim. Biophys. Acta 1505*, 185−208.
36. White, S. H., and Wimley, W. C. (1999) Membrane protein folding and stability: Physical principles, *Annu. Rev. Biophys. Biomol. Struct. 28*, 319−365.
37. Altschul, S. F., Gish, W., Miller, W., Myers, E. W., and Lipman, D. J. (1990) Basic local alignment search tool, *J. Mol. Biol. 215*, 403−410.
38. Berman, H. M., Westbrook, J., Feng, Z., Gilliland, G., Bhat, T. N., Weissig, H., Shindyalov, I. N., and Bourne, P. E. (2000) The Protein Data Bank, *Nucleic Acids Res. 28*, 235−242.
39. Thompson, J. D., Gibson, T. J., Plewniak, F., Jeanmougin, F., and Higgins, D. G. (1997) The ClustalX windows interface: Flexible strategies for multiple sequence alignment aided by quality analysis tools, *Nucleic Acids Res. 25*, 4876−4882.
40. Frishman, D., and Argos, P. (1995) Knowledge-based protein secondary structure assignment, *Proteins 23*, 566−579.
41. Humphrey, W., Dalke, A., and Schulten, K. (1996) VMD: Visual Molecular Dynamics, *J. Mol. Graphics 14*, 33−38.

42. Felsenstein, J. (2002) *PHYLIP (Phylogeny Inference Package)*, version 3.6a3, Department of Genome Sciences, University of Washington, Seattle (distributed by the author).
43. Sali, A., and Blundell, T. L. (1993) Comparative protein modeling by satisfaction of spatial restraints, *J. Mol. Biol. 234*, 779−815.
44. Laskowski, R. A., MacArthur, M. W., Moss, D. S., and Thornton, J. M. (1993) PROCHECK: A program to check the stereochemical quality of protein structures, *J. Appl. Crystallogr. 26*, 283−291.
45. Lovell, S. C., Davis, I. W., Arendall, W. B., III, de Bakker, P. I. W., Word, J. M., Prisant, M. G., Richardson, J. S., and Richardson, D. C. (2003) Structure validation by C-α geometry: ϕ, ψ, and C-β deviation. *Proteins 50*, 437−450.
46. Kalé, L., Skeel, R., Bhandarkar, M., Brunner, R., Gursoy, A., Krawetz, N., Phillips, J., Shinozaki, A., Varadarajan, K., and Schulten, K. (1999) NAMD2: Greater scalability for parallel molecular dynamics, *J. Comput. Phys. 151*, 283−312.
47. Melo, F., Devos, D., Depiereux, E., and Feytmans, E. (1997) ANOLEA: A www server to assess protein structures, *Intell. Syst. Mol. Biol. 97*, 110−113.
48. Zhang, L., and Hermans, J. (1996) Hydrophilicity of cavities in proteins, *Proteins 24*, 433−438.
49. McGuffin, L. J., Sodhi, J. S., Bryson, K., and Jones, D. T. (2004) Improving the Quality of Fold Recognition Models Using the nFOLD Methodology, Sixth Community Wide Experiment on the Critical Assessment of Techniques for Protein Structure Prediction, Gaeta, Italy.
50. Bamford, V., Bruno, S., Rasmussen, T., Appia-Ayme, C., Cheesman, M., Berks, B., and Hemmings, A. (2002) Structural Basis for the Oxidation of Thiosulfate by a Sulfur Cycle Enzyme, *EMBO J. 21*, 5599−5610.
51. Kadziola, A., and Larsen, S. (1997) Crystal structure of the dihaem cytochrome c_4 from *Pseudomonas stutzeri* determined at 2.2 Å resolution, *Structure 5*, 203−216.
52. Vandeyar, M., Weiner, M., Hutton, C., and Batt, C. (1988) A simple and rapid method for the selection of oligodeoxynucleotide-directed mutants, *Gene 65*, 129−133.
53. Cozzetto, D., and Tramontano, T. (2005) Relationship Between Multiple Seqeunce Alignments and Quality of Protein Comparative Models. *Proteins: Struct., Funct., Bioinf. 58*, 151−157.
54. Oh, J., and Kaplan, S. (2002) Oxygen Adaptation: The role of the CcoQ subunit of the cbb_3 cytochrome *c* oxidase of *Rhodobacter sphaeroides* 2.4.1, *J. Biol. Chem. 277*, 16220−16228.
55. Hendriks, J. H. M., Jasaitis, A., Saraste, M., and Verkhovsky, M. I. (2002) Proton and Electron Pathways in the Bacterial Nitric Oxide Reductase, *Biochemistry 41*, 2331−2340.
56. Puustinen, A., and Wikström, M. (1999) Proton exit from the heme-copper oxidase of *Escherichia coli*, *Proc. Natl. Acad. Sci. U.S.A. 96*, 35−37.
57. Qian, J., Mills, D. A., Geren, L., Wang, K., Hoganson, C. W., Schmidt, B., Hiser, C., Babcock, G. T., Durham, B., Millett, F., and Ferguson-Miller, S. (2004) Role of the Conserved Arginine Pair in Proton and Electron Transfer in Cytochrome *c* Oxidase, *Biochemistry 43*, 5748−5756
58. Seibold, S. A., Mills, D. A., Ferguson-Miller, S., and Cukier, R. I. (2005) Water Chain Formation and Possible Proton Pumping Routes in *Rhodobacter sphaeroides* Cytochrome *c* Oxidase: A Molecular Dynamics Comparison of the Wild-Type and R481K Mutant, *Biochemistry 44*, 10475−10485.
59. Mills, D. A., Geren, L., Hiser, C., Schmidt, B., Durham, B., Millett, F., and Ferguson-Miller, S. (2005) An Arginine to Lysine Mutation in the Vicinity of the heme Propionates Affects the Redox Potentials of the Hemes and Associated Electron and Proton Transfer in Cytochrome *c* Oxidase, *Biochemistry 44*, 10457−10465.
60. Wikström, M., Verkhovsky, M. I., and Hummer, G. (2003) Water-gated mechanism of proton translocation by cytochrome *c* oxidase, *Biochim. Biophys. Acta 1604*, 61−65.
61. Wikström, M., Ribacka, C., Molin, M., Laakkonen, L., Verkhovsky, M., and Puustinen, P. (2005) Gating of proton and water transfer in the respiratory enzyme cytochrome *c* oxidase, *Proc. Natl. Acad. Sci. U.S.A. 102*, 10478−10481.
62. Pereira, M. M., Verkhovskaya, M. L., Teixeira, M., and Verkhovsky, M. I. (2000) The caa_3 terminal oxidase of *Rhodothermus marinus* lacking the key glutamate of the D-channel is a proton pump, *Biochemistry 39*, 6336−6340.
63. Buse, G., Soulimane, T., Dewor, M., Meyer, H. E., and Bluggel, M. (1999) Evidence for a copper-coordinated histidine-tyrosine cross-link in the active site of cytochrome oxidase, *Protein Sci. 8*, 985−990.
64. Pfitzner, U., Odenwald, A., Ostermann, T., Weingard, L., Ludwig, B., and Richter, O. H. (1998) Cytochrome *c* Oxidase (Heme aa_3) from *Paracoccus denitrificans*: Analysis of Mutations in Putative Proton Channels of Subunit I, *J. Bioenerg. Biomembr. 30*, 89−97.
65. Pitcher, R. S., and Watmough, N. J. (2004) The Bacterial Cytochrome cbb_3 Oxidases, *Biochim. Biophys. Acta 1655*, 388−399.
66. Puustinen, A., Finel, M., Virkki, M., and Wikström, M. (1989) Cytochrome *o* (*bo*) is a proton pump in *Paracoccus denitrificans* and *Escherichia coli*, *FEBS Lett. 249*, 163−167.

BI060169A